JOURNAL OF COMPUTATIONAL PHYSICS 38, 157–184 (1980)

On Quantal Bound State Solutions and Potential Energy Surface Fitting. A Comparison of the Finite Element, Numerov–Cooley and Finite Difference Methods*

DAVID J. MALIK, JOSEPH ECCLES, AND DON SECREST

School of Chemical Sciences, University of Illinois, Urbana, Illinois 61801

Received August 10, 1979; revised November 30, 1979

This paper investigates several factors affecting the accuracy and efficiency of numerical determination of the bound state energy eigenvalues of the one dimensional Schrödinger equation. The efficiencies of the finite element method (FEM), the Numerov–Cooley method, and the finite difference method are compared. From this comparison, it is concluded that for potentials containing a single energy minimum, the Numerov–Cooley method is the most efficient, while for the most complex potentials the finite element method is superior due to its better numerical stability in the classically forbidden regions. The effects of various polynomial interpolation schemes on the calculated eigenvalues of potentials known only on a small number of points is examined. It is found that while higher order fits are superior to lower ones when the potential points are known accurately, they can introduce spurious information into the potential for inaccurately known points, and thus produce poor eigenvalues. Likewise, for accurately known potentials, a spline or Hermitian interpolation is better than a Lagrangian fit, but the Lagrangian functions are less susceptible to noise in a less well known case.

I. INTRODUCTION

The problem often arises of numerically solving the Schrödinger equation given the potential on only a discrete set of points. A priori potentials are difficult to compute accurately and usually are available only for a small set of points. In addition, these points are usually known only over a small "important" range of separations. The potential must be interpolated in some manner and extrapolated to regions not given explicitly by potential points and their interpolation [1–3]. This paper discusses and evaluates fits to a priori potentials and subsequent numerical solution of the eigenvalue problem.

Numerous techniques exist in the literature for solving the Schrödinger equation numerically [1, 4–7]. An adaptation of the finite element method (FEM) is given here which has the properties of being efficient and easily applicable to any potential. This

* Supported in part by a grant from the National Science Foundation.

0021-9991/80/140157–28$02.00/0

method is compared with several others and its advantages and disadvantages discussed.

The finite element method has had extensive application in engineering problems [8, 9]. Only recently has it been brought into the sphere of quantum mechanics by Askar, who has applied the method to the calculation of the bound states of the hydrogen atom using linear interpolation functions [10]. Nordholm and Bacskay have presented a variation of FEM for bound and continuum state problems [11, 12]. More recently Askar *et al.* have applied the FEM to the collinear reactive scattering of $H + H_2$ [13]. In the FEM formulation for the bound state problem, the Schrödinger equation becomes a generalized algebraic eigenvalue problem. In addition, it is easily extended to multiple dimensions. This has been utilized by Friedman *et al.* in the solution of the two dimensional Schrödinger equation [14].

In Section II the finite element method for bound state solutions to the Schrödinger equation is discussed and an efficient algorithm is presented for the solution of the resulting generalized eigenvalue problem. The accuracy and convergence properties of the method are discussed. The efficiency of FEM is also compared with that of other methods. In Section III, the use of interpolating polynomials and various extrapolating forms for potentials are investigated. A summary of the results is provided in Section IV.

II. The Finite Element Method

The FEM is simple and straightforward for the one dimensional eigenvalue problem. It can be cast into a form resembling the Rayleigh-Ritz variation method. Since the complete method is given elsewhere [15, 16], it will only be outlined here.

The radial or one dimensional Schrödinger equation may be written

$$\psi'' + [E - V(r)]\psi = 0. \tag{1}$$

The bound state boundary conditions are simply $\psi(r) = 0$ at $r = r_a$ and $r = r_b$, where r_a and r_b are the boundaries of the region. If Eq. (1) is multiplied by $\psi(r)$ and integrated once, an equivalent form is obtained,

$$\psi(r_b)\,\psi'(r_b) - \psi(r_a)\,\psi'(r_a) = -\int \psi'(r)^2\,dr + \int \psi(r)\,\sigma(r)\,\psi(r)\,dr, \tag{2}$$

where $\sigma(r) = E - V(r)$. The first term in Eq. (2) is zero due to the boundary conditions. If r_a and r_b are far enough into the classically forbidden region of the potential, then these boundary conditions will correspond closely to the physically correct ones. The functional which will be extremized using a suitable basis set is given by

$$I[\psi] = -\int [\psi'(r)]^2\,dr + \int \psi(r)\,\sigma(r)\,\psi(r)\,dr. \tag{3}$$

In distinction to the usual choices of basis functions, which are globally defined, one chooses a basis set with functions which are non-zero over only small regions, or elements. These functions must satisfy certain continuity and completeness conditions, which will be discussed later.

The wavefunction is expanded in the basis functions as,

$$\psi(r) = \sum_i C_i N_i(r), \tag{4}$$

where the C_i are the coefficients and the N_i are interpolation functions. (A possible set of such functions are described in detail in Appendix A.) The index i denotes the associated node which is related to a spatial point in the region of interest. If Eq. (4) is substituted into the functional $I[\psi]$, one obtains

$$I[\psi] = \sum_{i,j} C_i C_j \int (N_i(r)\, \sigma(r)\, N_j(r) - N_i'(r)\, N_j'(r))\, dr. \tag{5}$$

This expression can be extremized in the usual way by evaluating the variation in I with respect to C_j, and equating to zero. The resulting equation can be written

$$\sum_i (H_{ji} + ES_{ji})\, C_i = 0, \tag{6}$$

where

$$H_{ji} = \int [H_j(r)\, V(r)\, N_i(r) - N_j'(r)\, N_i'(r)]\, dr, \tag{7}$$

and

$$S_{ji} = \int N_j(r)\, N_i(r)\, dr. \tag{8}$$

Since S_{ji} is not diagonal, this is a generalized eigenvalue problem. Techniques for solving the system are discussed later in this section and in the appendices.

An important feature of the functional in Eq. (5) is the absence of the second derivative. Consequently, the requirements on the trial functions for the functional are less stringent than for the original Schrödinger equation, Eq. (1).

As was previously stated, the boundaries are chosen sufficiently into the classically forbidden region so that neglect of the left-hand side of Eq. (2) is valid. This region between r_a and r_b can then be divided into intervals or elements, not necessarily of equal size. In two dimensions, the elements can be triangular, rectangular, or whatever shape is appropriate to the region. Curved boundaries are also treatable, although they may complicate the evaluation of the necessary surface integrals over the elements.

Once the geometry is specified, integrals are evaluated analytically over the

elements. For the overlap integral, S_{ji}, and the kinetic energy integral, $\langle N_j' | N_i' \rangle$ can be evaluated analytically given the form of N_i. For the potential integral, $\langle N_j | V | N_i \rangle$, the evaluation must normally be numerical. In addition, since this integral is dependent on the potential, it varies from element to element.

Excess error can be introduced into this procedure in several ways. One is a poor choice of the region of integration; that is, the region does not sufficiently penetrate the non-classical region of the potential. Another is the use of excessively large elements.

Usually the functions are chosen to be simple piecewise polynomials with certain continuity and completeness properties. A convenient choice for these polynomials are Lagrangian or Hermitian interpolates, with the property,

$$N_i(r_j) = \delta_{ij}, \tag{9}$$

where δ_{ij} is a kronecker delta. Hence $\psi(x_i)$ is simply C_i, which provides direct physical significance for the coefficients determined by the solution of Eq. (6). The condition specified by Eq. (9) also provides the necessary continuity requirements for the interpolation functions. This is described in greater detail by the example below.

The functions N_i are associated with nodes i, the number of which in one element is determined by the polynomial degree. For example, if there are nodes only at the endpoints of the element, the lowest order uniquely defined polynomial is linear. If a third node is added to the element, a quadratic polynomial is used. For five nodes per element a fourth order Lagrangian interpolate could be employed. If Hermitian interpolates are to be used, specifying both function and derivative at the nodes, then a cubic function would be used in a two node element. These functions are termed interpolation functions since they provide the solution between the nodes given the coefficients C_i, which are the solution at the nodes.

An example will clarify the nodal structure and the significance of Eq. (9). Consider the quadratic interpolate case of five nodes numbered consecutively, and divided into two elements:

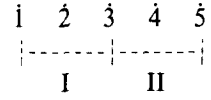

The nodes (numbered 1–5) are associated with elements (numbered I and II) with node 3 being shared by both elements. Interface nodes are called primary and interior nodes are called secondary. The polynomials N_i will be quadratic Lagrangian interpolates that satisfy Eq. (9). Between nodes 1 and 3, N_2 will be non-zero, but unity at 2. N_1 is unity at 1 and zero at nodes 2 and 3. The interpolates are defined only on the element containing the node, so that N_4 and N_5 will be zero in the first element. Note, though, that N_3 is non-zero in both elements, but not beyond. Hence for $r_1 < r < r_3$, the solution is given by,

$$\psi(r) = C_1 N_1(r) + C_2 N_2(r) + C_3 N_3(r). \tag{10}$$

One should note that the functional form of $N_3(r)$ is different in elements I and II. In order to maintain continuity at the element interface, the interpolate property given by Eq. (9) is crucial. Note that for $r = r_3$, both $N_1(r_3)$ and $N_2(r_3)$ are zero and $N_4(r_3)$ and $N_5(r_3)$ are zero. This interpolate property ensures continuity across the element interface without adding any additional equations to the system of Eq. (6). In Appendix A the Lagrangian interpolates are given for the linear case, and extension to higher order is described.

The kinetic energy and overlap integrals of Eqs. (8) and (9) can be evaluated easily from the analytic form of the interpolates. However, the potential integral is not in general amenable to analytic treatment. The potential can be approximated, however, by an interpolation of the values at the nodes. For instance, in element I of the system shown above the potential becomes,

$$V(r) = V(r_1)\, N(r_1) + V(r_2)\, N_2(r) + V(r_3)\, N_3(r). \tag{11}$$

Substituting this into the potential integral of Eq. (7) reduces this integral to a weighted sum of integrals of the form $\langle N_i | N_k | N_j \rangle$, which can be evaluated analytically. This process simplifies the computation of the spatially dependent potential integrals. A further approximation has thus been introduced into the procedure.

The assembly of the integrals is straightforward. Each node is considered sequentially, and all node couplings are accumulated in two matrices, H and S. Consider again the two element, five node example. Note that node 3 has contributions from both elements. Thus, in addition to H_{33}, the elements H_{31}, H_{32}, H_{34}, and H_{35} are non-zero.

The boundary conditions for the bound state problem may be incorporated into the matrix by omitting the nodes at the endpoints of the potential region, which is the equivalent to equating the coefficients at those points to zero. The remaining nodes are zero at these endpoints by virtue of the definition in Eq. (9).

A. *Convergence Properties and Errors in the Finite Element Method*

The convergence properties of the finite element method have been extensively studied. As with any numerical method the convergence tests must be implemented in a consistent way to obtain correct solutions. Solutions may appear converged, but may in fact converge to an erroneous solution. With the FEM, solutions are tested in two ways: (i) the given mesh is successively refined, or (ii) for a specified mesh scheme, the degree of the interpolating polynomial is increased. These tests in themselves, however, do not assure a correctly converged solution unless both the elements and interpolation functions satisfy certain criteria. These requirements will be discussed later in this section.

First we consider convergence by element reduction. Refinement of the mesh must occur in a regular fashion. All the mesh schemes must also possess the same boundaries in the potential region of interest. In order to investigate the convergence of the wavefunction, each successive refinement must possess a subset of the nodal structure

from previous node schemes. Hence each successive scheme retains all the previous nodes. This is neccessary because, as will be shown, the error between the nodes is generally larger than that at the nodes, and meaningful convergence criteria can be given only for nodal values.

Interpolation functions N_i must also satisfy certain specific requirements of completeness and compatibility. The *completeness* condition requires that the interpolating polynomial be of at least degree k, where k is the highest order derivative of the variable in the functional. Hence the functional within an element is defined both in terms of the variable and its derivatives. If the element size now approaches zero, the function approaches the true solution. If a higher degree polynomial is used, one can in general expect that the convergence will be more rapid.

Compatibility requires that the solution and its derivatives up to $(k-1)$th order be continuous across elemental interfaces. This condition is sometimes called element conformity. For the functional in Eq. (5) only continuity of the approximate solution is required. If a discontinuity occurs in the derivative, the integrals can still be integrated and no problem is presented.

Several factors may prevent a true quantum mechanical solution. However, in a numerical sense the solution can be made exact to an arbitrary degree of accuracy. The error contribution from round-off will not be considered, and instead the errors introduced by the method itself will be examined. In general the errors can be divided into three classes:

1. discretization errors;
2. numerical integration errors; and
3. interpolation errors.

Discretization errors occur since for any realistic potential the relevant region of space is of infinite extent and cannot be accounted for by a finite number of elements. Since the wavefunction is not in fact zero beyond the integration limits chosen, an error results. This can be reduced by extending the region treated further into the classically forbidden region.

In most cases the potential integral is too complicated to evaluate analytically, and numerical quadrature is more convenient. This introduces an integration error.

The last source of error depends on the type of interpolation function used. If N_i is a degree m polynomial ($m \geqslant k$), the order of error in the interpolation is of order h^{m+1}, where h is the element size (for equal elements). However, this is not the error in either the eigenfunctions or the eigenvalues. It has been shown elsewhere that the error in eigenvalues is of order h^{2m}, where m is the order of the interpolate [15]. Both integration and interpolation errors are reduced by increasing the number of elements, thereby reducing h.

The wavefunctions for the Morse oscillator,

$$V(r) = 4(1 - e^{-r/2})^2, \tag{12}$$

have been calculated using FEM and have been compared to the analytic solutions. The absolute errors have been plotted in Fig. 1 for the lowest two states. The results were obtained using 30 element (89 node) and 60 element (179 node) regions with cubic Lagrangian interpolates. The integration boundaries were $r = -4$ and $r = 13$; for $r \leqslant -4$ and $r \geqslant 13$, the approximate solution is equated to zero. As can be seen in plate d, and less visibly in plate b, the discretization error in the wavefunction is greatest near the boundary points. The error beyond each cusp (at $r = -4$ and $r = 13$) is identically the exact wavefunction. The magnitude of the error at each cusp could be reduced by extending the endpoint further into the non-classical region. The discontinuity of the derivative between elements is clearly indicated in the figure. The thin line shows the error of the Lagrangian interpolated wavefunction, while the heavy line is that for a spline fit of all the nodes. The spline fit has the benefit that the discontinuities in the derivative at element interfaces are eliminated and internode error of the wavefunction is reduced. A close inspection reveals that the primary node error is usually less than that at the secondary nodes. If a spline fit to just the primary nodes is used, however, the maximum error is nearly an order of magnitude greater than the error shown by the heavy line. The wavefunction error increases for the excited states since more nodes are required to describe the increased curvature.

The eigenvalues obtained from these calculation are a function of the number of

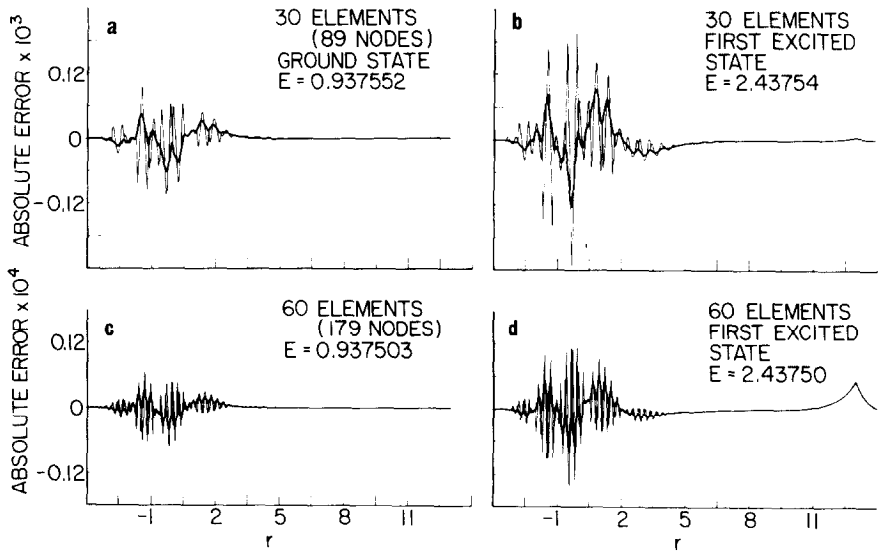

FIG. 1. The absolute error in the FEM wavefunction for the Morse potential, Eq. (12): (a) the ground state error for a 30-element calculation; (b) the first excited state error for 30 elements; (c) the ground state error for 60 elements; (d) the first excited state error for 60 elements. It should be noted that the error scales in the lower plates are an order of magnitude less than those above. The light line is the cubic Lagrangian error and the heavy line is the error of the spline fit to the primary and secondary nodes. The integration limits are $r = -4$ and 13.

elements n. The true eigenvalue to which these converge can be written as a power series in $1/n$ as

$$E_v^{(\infty)} = E_v^{(n)} + \sum_j a_{vj}/n^{2(m+j)}, \tag{13}$$

where m is the order of the interpolating function [15]. If all but the first few terms are negligible, then a knowledge of $E_v^{(n)}$ for several n's provides a set of simultaneous equations which can be solved for $E_v^{(\infty)}$. This process, Richardson extrapolation, is used to improve the accuacy of the FEM results.

B. *Efficiency of the Finite Element Method*

The FEM algorithm was coded in FORTRAN for a CDC CYBER 175 using linear, quadratic, and cubic Lagrangian polynomials. The cubic version was found to be the most accurate and efficient, and was used in all the calculations reported here. This implies that in a calculation performed using n elements, the potential, and subsequently the wavefunction, were evaluated at $(3n-1)$ nodes. The efficiency was compared to that of the finite difference method [6] and the Numerov–Cooley method [4]. Wicke and Harris [1] have found the Numerov–Cooley integration method to be more efficient than either the finite difference or the Harris–Engerholm–Gwinn (HEG) variational method. However, Numerov integration encounters stability problems when one integrates into a classically forbidden region, and so modifications must be made in the case of double minimum potentials to allow the Numerov–Cooley method to work. Such a problem does not occur with the finite element, finite difference, or HEG methods.

The Numerov–Cooley approach is an iterative one and requires an initial guess of the eigenvalues. In the program used here, the first guess of the ground state is assumed to be the value of the potential at the equilibrium position. This quickly converges to the lowest eigenvalue. After a converged ground state eigenvalue is obtained, a harmonic oscillator approximation is used to provide guesses for the higher eigenvalues. When a converged result is obtained, the nodes are counted. If any states are missing intermediate guesses are made, until all states are found.

The FEM and Numerov–Cooley programs used here have been made available through QCPE [17].

The comparison of execution times was carried out for the calculation of the lowest 31 eigenvalues and eigenvectors of a Morse potential with $\omega_e = 1000\ \text{cm}^{-1}$ and $\omega_e x_e = 8\ \text{cm}^{-1}$. For the potential used here, the equilibrium position was 1.5 atomic units, and the boundaries were at 0.0 and 9.0 atomic units. The discretization error was less than one part in 10^{-8} in the $v = 30$ eigenvalue. The calculations were carried out at two levels of accuracy, the first requiring that the uppermost eigenvalue ($v = 30$) be accurate to 10^{-8}, the second requiring that this eigenvalue have a relative error of no more than 10^{-4}. Table I summarizes the timing data. For the first set of calculations, the FEM results were produced with a 60 element (179 node) direct calculation, followed by a 65, a 150 and a 500 element (194, 449, and 1499 node)

TABLE I

Execution Times at Several Levels of Accuracy of Calculating the $v = 0$–30 Eigenstates of a Morse Oscillator[a]

	Method		
Relative Accuracy	Numerov–Cooley	FEM	Finite differences
1. −8 for $v = 30$	(1.0 −3)[b] 3.014 sec	(1.8 −3) 11.781 + 21.406 = 33.187 sec[c]	(2.0 −3) 73.168 sec
1. −4 for $v = 30$	(7) 0.971 sec	(2) 11.781 + 7.793 = 19.574 sec	(6) 35.983 sec

[a] Eigenvalues are in units of cm^{-1}.

[b] Numbers in parentheses are the absolute error in $v = 30$. The notation a −n means $a \times 10^{-n}$. The exact eigenvalue is 23,058.

[c] For the FEM results, the upper two numbers represent the time for the direct solution to obtain an initial guess and the iterative refinement, respectively. The lower number is the sum.

iterative calculation, and Richardson extrapolation of the 150 and 500 element results. The result had an error of 0.002 in the $v = 30$ state. The true eigenvalue is 23,058 cm^{-1}. The Numerov–Cooley results required a 500 and a 2000 node calculation, which left an error of 0.001 cm^{-1}. While this is more than the total number of nodes necessary for FEM, the execution time can be seen to be more than an order of magnitude less. The finite difference calculation was based on a Richardson extrapolation of 500, 1000, 2000, and 2500 node results. The error in the highest eigenvalue was −0.003. The lower-accuracy results for FEM were performed with 60, 65, and 175 element calculations, with extrapolation of the 65 and 175 element cases, and giving an error of 2 cm^{-1} in $v = 30$. Numerov–Cooley used a single 500 node calculation, with an error of 7 cm^{-1}. Finally the low-accuracy finite difference calculation used extrapolation from 1000 and 2000 nodes, and the error was 2 cm^{-1}.

There are two additional points to be noted from these results. The first is that in this case the potential was relatively simple and required little evaluation effort. If a very complex potential were being investigated, the finite difference method would be even less efficient relative to the other two. For high accuracy, this would make little difference between the FEM calculations, which required 2321 potential evaluations, and the Numerov–Cooley, which required 2500. For the lower accuracy, the efficiency of Numerov–Cooley is enhanced since it needs 500 evaluations compared with 897 for FEM. The optimal scheme of using each of the methods varies due to the differing order of error in step-size of each of the formulations: second order for finite difference, fourth for Numerov–Cooley, and sixth for FEM. The low order errors in finite difference calculations cause larger error, and make it an ideal candidate for extrapolation, as described earlier. The other two methods are less

improved by the use of extrapolation since they already contain less error. For a fixed total number of nodes in a series of calculations, the optimal extrapolation scheme differs for finite differences and Numerov–Cooley or FEM. For finite differences the points should be distributed over several varying step sizes. For Numerov–Cooley and FEM only two calculations need be used for the extrapolation.

The Numerov–Cooley method is clearly shown to be the most efficient of the methods tested. Thus, for *single* minimum potentials, where no numerical instability is expected, Numerov–Cooley is the best method to employ. For *multiple* minimum potentials, where Numerov–Cooley is known to have problems, one of the matrix methods would be more appropriate. FEM can be seen to be superior to finite differences.

III. The Potential Fitting Problem

The potential fitting problem can be succinctly stated. Given a set of a priori values of the potential, find a potential function which is suitable for use in computing the eigenvalues and eigenvectors of the potential. This entails interpolation between the known points and extrapolation beyond their range. Thus there are two problems to consider. Extrapolation beyond the a priori points is difficult and is most reliably accomplished by the used of additional information. This problem will be treated later. First we shall consider the problem of interpolation. For this purpose the exact potential function is used beyond the range of the tabulated points.

As has been pointed out by Truhlar and Tarara, the interpolation of a potential energy surface is an important consideration in bound state eigenvalue problems [3]. The form of the interpolating function can introduce differences in the potential sufficient to make quite noticeable changes in the calculated eigenvalues. Often a potential surface will be computed only in the vicinity of the minimum and must be extrapolated to large and small distances. It is important to know how critical the long-range behavior of the potential is to the accuracy of eigenvalues.

A common type of interpolating function is a piecewise polynomial of degree m. The three most widely used forms are Lagrangian interpolates, Hermitian interpolates, and spline functions. Lagrangian interpolates are determined by the tabulated values of the potential at $m + 1$ points in the vicinity of the point to be evaluated. Hermitian interpolates require a knowledge of the values of both the function and its derivative at $(m + 1)/2$ points, and thus can exist only for odd order m. Both Hermitian and Lagrangian interpolates are defined by only a small number of points adjacent to the point of evaluation. In contrast spline functions are global functions: the fit at any point is affected by all of the tabulated points, although the nearby points are the most important. The spline is completely determined by the set of functional values, the continuity of the function and its lowest $m - 1$ derivatives, and the specification of $(m - 1)/2$ derivatives at the two endpoints of the spline region. Like Hermitian interpolates, spline functions are always of odd order.

A. *Morse Potential*

Truhlar and Tarara investigated interpolation accuracy using the Kołos and Wolniewicz $E, F^1\Sigma_g$ potential of H_2 [2]. The error was difficult to assess due to the fixed number of potential values available. It would be advantageous to have a better measure of the accuracy of interpolation. This can be accomplished by interpolating points generated from an analytic potential, which has accurately known eigenvalues. The potential used here is a Morse oscillator, given by Eq. (12), which has four bound states with eigenvalues 0.9375, 2.4375, 3.4375, and 3.9375.

The region between $r = -2$ and $r = 6$ was evaluated as an interpolation of n equispaced points for $n = 5$, 9, 17, and 33. The interpolation functions were third and fifth order Lagrangian, Hermitian, and spline functions. The number of points were chosen such that the true potential minimum was at one of the known points. This is consistent with the application of the information gained in this study to the fitting of ab initio potential surfaces, since the values of the potential in the region around the quilibrium position are generally well known.

The calculation for this series of potentials was done with a Numerov–Cooley program. The integration limits were from $r = -3.5$ to $r = 50.0$. The step size was about 0.107, corresponding to 500 nodes. This was sufficient to produce an accuracy of 9 to 10 figures for all four states.

Tables II–IV show the eigenvalues for the interpolated potentials. The results are converged to a relative accuracy better than 10^{-9}, and thus all of the error is the result of error in the interpolated potential. In all cases the interpolated potential has eigenvalues which seem to converge as more points are added. A fifth order

TABLE II

Eigenvalues for Lagrangian Interpolation of Discrete Morse Potential Points between $r = -2$ and $r = 6$[a]

	Number of discrete points (spacing)			
v	5(2.)	9(1.)	17(0.5)	33(0.25)
0	0.74659300[b]	0.89290445	0.93457054	0.93731721
	—	0.93905219	0.93764981	0.93750260
1	2.52672956	2.41527342	2.43553495	2.43737193
	—	2.43712370	2.43758170	2.43750179
2	3.51852238	3.42913581	3.43640478	3.43742491
	—	3.43800754	3.43753771	3.43750104
3	3.96196219	3.93552190	3.93714686	3.93747503
	—	3.93794932	3.93751095	3.93750034

[a] Exact Morse potential outside this range. Eigenvalues are in the reduced units of Eq. (1).

[b] The upper number in each set is for third order interpolates, while the lower is for fifth order.

TABLE III

Eigenvalues for Hermitian interpolation of Discrete Morse Potential Points between $r = -2$ and $r = 6$[a]

	Number of points (spacing)			
v	5(2.)	9(1.)	17(0.5)	33(0.25)
0	0.85814285[b]	0.93310309	0.93723218	0.93748336
	0.92728313	0.93726550	0.93749553	0.93749992
	0.91414007	0.93693403	0.93749285	0.93749990
1	2.36291032	2.43436574	2.43730904	2.43748814
	2.42830638	2.43733260	2.43749681	2.43749994
	2.42030243	2.43714476	2.43749497	2.43749993
2	3.38908722	3.43563016	3.43738564	3.43749290
	3.43085672	3.43739988	3.43749809	3.43749997
	3.42520334	3.43731291	3.43749704	3.43749996
3	3.92139765	3.93687240	3.93746151	3.93749761
	3.93524784	3.93746668	3.93749936	3.93749999
	3.93383135	3.93744239	3.93749902	3.93749999

[a] Exact Morse potential used beyond this range. Eigenvalues are in the reduced units of Eq. (1).

[b] Top number of each group is for third order interpolation, while the bottom two are for fifth order. The center result is for interpolation based on the two points around the point to be evaluated plus the next discrete point at higher r. The bottom number is for the potential where the extra point is at lower r.

TABLE IV

Eigenvalues for Spline Function Interpolation of Discrete Morse Potential Points between $r = -2$ and $r = 6$[a]

	Number of points (spacing)			
v	5(1.)	9(1.)	17(0.5)	33(0.25)
0	0.89353476[b]	0.93464959	0.93725140	0.93748367
	0.93430712	0.93756260	0.93750153	0.93750003
1	2.34589297	2.43571085	2.43732272	2.43748835
	2.44407468	2.43755196	2.43750109	2.43750002
2	3.38701324	3.43619145	3.43739383	3.43749302
	3.44052716	3.43753100	3.43750066	3.43750001
3	3.92063250	3.93699585	3.93746423	3.93749765
	3.93858868	3.93750998	3.93750022	3.93750000

[a] Exact Morse potential used outside of this range. Eigenvalues are in the reduced units of Eq. (1).

[b] The upper number in each set is for the third order interpolation, while the lower is for fifth order.

Lagrangian fit does not exist for five points because at least six points are required. Note that for higher quantum numbers there is a decrease not only in the relative error, but also in the absolute error in all cases. This reflects the fact that the wavefunction depends upon the quantity $E - V(r)$, and as E becomes large, small errors in V have less effect on the form of the function. A second important feature is the accuracy for different interpolation methods. For each type of fit the fifth order gives better results than the third. The Lagrangian fits produce the worst results in each case. The error in the spline function and Hermitian interpolations are very similar, with the spline results being just slighly better in most cases.

The implication seems to be that spline or Hermitian interpolation schemes are preferable to Lagrangian ones. The spline functions have a definite advantage over the Hermitian interpolates in that they do not require a knowledge of the derivatives at all points. They do require $(m-1)/2$ derivatives at the outermost points, but the fit is very insensitive to small errors in these values, and numerical evaluation of these derivatives is quite satisfactory. Higher order splines suffer from a stability problem in evaluation, and are not in widespread use. Recent work on the evaluation of higher order splines has made accurate evaluation possible [18].

B. *Kołos and Wolniewicz E, $F^1\Sigma_g$ Potential for H_2*

It should be noted that the results presented above are obtained from a "noiseless" potential; that is, the potential is known exactly at the tabulated points. The normal case for the fitting of an ab initio potential surface is different in that the tabulated points are known only inexactly and contain noise from such sources as roundoff, basis set truncation, etc. The properties of "noisy" functions are harder to characterize (see, for example, [19]). For these cases "exact" results are not available. The H_2 potential of Kołos and Wolniewicz mentioned earlier provides an example. This potential has been investigated by Lin [20], Tobin and Hinze [21], Wolniewicz and Orlikowski [22], and Truhlar and Tarara [3]. As has been pointed out by Truhlar and Tarara the disagreement between the various sets of calculations are to a large extent due to differences in interpolation. The results of the present investigation are listed in Tables V and VI. Table V gives eigenvalues for the potential utilizing all points given by Kołos and Wolniewicz. Fifteen points in this set are closely spaced around the extrema. Table VI presents results for the potential evaluated without those 15 points. The discrepancy between the two sets of results with and without the 15 points is much more pronounced for the fifth order interpolation than for the third. Since these 15 points are all in the vicinity of the extrema of the potential and since the effect of differences in these points will be local to these regions, we will concentrate on examining the potential in these areas.

As shown in Figs. 2–5, the fifth order interpolates have some difficulty in handling the unevenly spaced points near the minima. The most noticeable problems are with the fifth order spline at the inner minimum, and with both the fifth order spline and fifth order Hermitian interpolates at the outer minimum. The fifth order spline produces a substantial oscillation around the outer minimum, while in the other two cases the depth of the minimum is increased and its position slightly shifted. The fifth

TABLE V

Eigenvalues (cm^{-1}) for Various Fits of the Kołos and Wolniewicz $E, F^1\Sigma_g$ Potential for H_2[a]

	Cubic fits			Fifth order fits		
v[b]	Lagrangian	Hermitian	spline	Lagrangian	Hermitian	spline
0−	1234.3596	1236.2993	1235.9635	1234.1353	1236.2650	1264.3831
1+	1410.0356	1409.8164	1409.7057	1410.3300	1379.5394	1390.9212
2+	2605.4701	2604.9767	2604.8131	2604.5785	2600.3336	2588.9568
3−	3560.4542	3564.1103	3564.1950	3564.4195	3564.1700	3555.6382
4+	3744.3607	3743.4521	3743.2700	3743.4056	3737.6163	3720.7413
5+	4816.8434	4815.3089	4815.3309	4815.5052	4804.6423	4817.9244
6−	5587.0974	5589.5919	5590.6232	5589.6497	5589.5040	5605.2988
7+	5890.5907	5890.8536	5891.2727	5890.9854	5890.1172	5888.1878
8+	6749.8062	6750.1432	6750.6155	6750.8575	6744.6168	6748.8532
9−	7422.9190	7425.1974	7426.4895	7425.1265	7424.5624	7418.1941
10+	8045.3825	8047.1984	8048.8814	8047.5100	8041.9893	8042.3993
11+	8779.574	8781.431	8783.041	8781.913	8780.411	8776.992
12−	9502.634	9504.942	9506.777	9505.327	9501.939	9506.398
13+	10201.05	10203.27	10205.45	10203.71	10200.10	10208.05
14	10900.95	10902.86	10905.09	10903.50	10902.31	10910.24
15	11598.42	11600.39	11602.30	11600.90	11595.92	11605.97
16	12282.54	12284.44	12286.01	12284.65	12283.02	12287.77
17	12950.81	12952.44	12953.92	12952.81	12951.60	12952.92
18	13604.89	13606.05	13607.32	13606.52	13602.15	13604.12
19	14244.22	14254.11	14245.83	14245.39	14243.19	14243.27
20	14866.83	14867.50	14867.76	14867.80	14867.34	14866.24
21	15471.45	15471.95	15471.60	15472.24	15469.72	15470.37
22	16057.38	16057.53	16056.43	16057.77	16054.37	16055.52
23	16623.96	16623.66	16621.79	16623.77	16622.54	16621.16
24	17169.91	17169.21	17167.36	17169.51	17168.98	17167.08
25	17693.85	17693.02	17692.60	17693.95	17691.99	17693.93

[a] All reported points are used.

[b] Those states marked as (+) have greatest density in the outer minimum, while those marked as (−) are mainly in the inner minimum.

order Lagrangian fit provides an irregular shape evident at both minima, although not as pronounced as in the other two cases.

Apparently higher order interpolation schemes become more sensitive to extraneous noise in the tabulated function. Caution is needed in applying such methods to ensure that spurious structure is not introduced into the function by the interpolation process. In the region near a potential extremum any closely spaced points will be close in functional value, and a small amount of noise can become a substantial portion of the change in values between the points. Thus higher order

TABLE VI

Eigenvalues (cm^{-1}) for Various Fits of the Kołos and Wolniewicz $E, F^1\Sigma_g$ Potential fr H_2[a]

	Cubic fits			Fifth order fits		
v[b]	Lagrangian	Hermitian	spline	Lagrangian	Hermitian	spline
0−	1234.2336	1236.2766	1235.9387	1236.5146	1236.2591	1229.5402
1+	1410.0178	1409.8162	1409.7535	1409.5982	1409.6810	1409.6937
2+	2605.4620	2604.9754	2604.8469	2604.6197	2604.8461	2604.9062
3−	3560.4227	3564.1060	3564.1853	3564.4614	3564.2067	3560.0404
4+	3744.3040	3743.4448	3743.2714	3743.2595	3743.3678	3743.3584
5+	4816.5883	4815.2735	4815.2415	4815.4554	4815.0683	4814.9242
6−	5586.2915	5589.4802	5590.3357	5590.0220	5589.7221	5597.0888
7+	5890.4057	5890.8288	5891.2664	5891.3464	5890.7614	5894.3733
8+	6748.5083	6749.9614	6750.2746	6750.4918	6750.1801	6754.2754
9−	7421.7182	7425.0273	7426.0356	7425.1272	7425.3908	7439.9870
10+	8045.3034	8047.1903	8048.8948	8047.9720	8047.2959	8065.2530
11+	8778.735	8781.312	8782.840	8781.738	8781.556	8799.763
12−	9501.642	9504.798	9506.392	9504.810	9505.130	9527.923
13+	10200.80	10203.24	10205.40	10203.79	10203.34	10230.03
14	10900.78	10902.84	10905.08	10903.63	10902.81	10930.00
15	11597.81	11600.30	11602.05	11600.64	11600.44	11626.89
16	12281.89	12284.34	12285.76	12284.41	12284.52	12310.08
17	12950.52	12952.40	12953.89	12952.90	12952.40	12976.28
18	13604.79	13606.04	13607.36	13606.80	13605.99	13626.52
19	14243.97	14245.08	14245.74	14245.56	14245.08	15261.10
20	14866.37	14867.44	14867.55	14867.77	14867.48	14878.82
21	15471.00	15471.88	15471.42	15472.17	15472.02	15478.17
22	16057.10	16057.49	16056.38	16057.80	16057.43	16058.19
23	16623.83	16623.64	16621.82	16623.86	16623.59	16618.95
24	17169.81	17169.20	17167.37	17169.55	17169.11	17161.38
25	17693.67	17693.00	17692.54	17693.89	17693.43	17686.18

[a] Fifteen of the points reported were not used, as noted by Truhlar and Tarara [3].

[b] Those states marked as (+) have greatest density in the outer minimum, while those marked as (−) are mainly in the inner minimum.

interpolation schemes are forced to take on unreasonable forms to match these changes.

Since the various interpolation schemes work well for exactly known potentials, as pointed out earlier, lack of agreement among them is as much an indication of the worth of the tabulated points as of the suitability of one method of interpolation or another. The Morse oscillator calculations show that the Hermite or spline interpolation gives better results than the Lagrangian, and that the higher order is

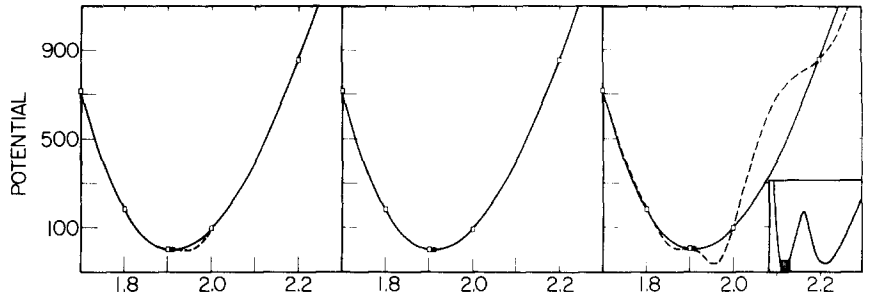

FIG. 2. The interpolated inner minimum of the Kołos and Wolniewicz $E, F^1\Sigma_g$ potential of H_2. Shown are Lagrangian (left panel), Hermite (center), and spline (right) interpolation. Both third (solid line) and fifth (dashed line) order functions were used. The two lines are indistinguishable in the center panel. All points reported by Kołos and Wolniewicz were used. The tabulated points are shown as □. The filled circle at the bottom represents six points too close to resolve on this scale. The shaded box within the small inset shows the location of these panels within the potential. The potential is given in units of cm^{-1}.

preferable, at least for potentials with low noise levels. The splines enjoy an advantage over the Hermitian interpolates in that there is no need to have the tabulated values of the derivatives at each point.

It is emphasized that a "black-box" interpolation scheme is dangerous, and that the results of interpolation should be carefully scrutinized before they can be trusted. A reasonable scheme would be to apply both third and fifth order splines, and consider a lack of agreement between the two to indicate a lack of smoothness in the tabulated function. A visual inspection of the interpolated function would show if any spurious oscillations were present in one or both cases. An inspection of the fit potential would suggest which points should be refined or discarded. Refinement might imply recalculation of the points with greater accuracy, or a smoothing of the points in that

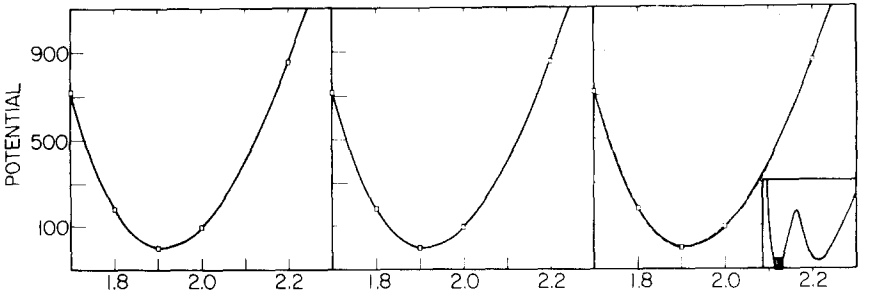

FIG. 3. The interpolated inner minimum of the Kołos and Wolniewicz $E, F^1\Sigma_g$ potential of H_2. Shown are Lagrangian (left panel), Hermite (center), and spline (right) interpolation. Both third (solid line) and fifth (dashed line) order functions were used, but only in the case of the spline fits are the curves distinguishable. Fifteen points clustered around the extrema have been deleted, as described in the text. The tabulated points are shown as □. The shaded box within the small inset shows the location of these panels within the potential. The potential is given in units of cm^{-1}.

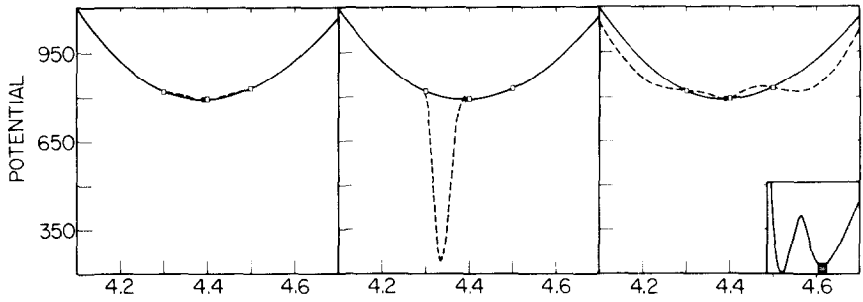

FIG. 4. The interpolated outer minimum of the Kołos and Wolniewicz $E, F^1\Sigma_g$ potential of H_2. Shown are Lagrangian (left panel), Hermite (center), and spline (right) interpolation. Both third (solid line) and fifth (dashed line) order functions were used. All points reported by Kołos and Wolniewicz were used. The tabulated points are shown as □. The filled circle at the bottom represents six points too close to resolve on this scale. The shaded box within the small insert shows the location of these panels within the potential. The potential is given in units of cm^{-1}.

region. The agreement of the various types of fit with appropriate points discarded gives an idea of the maximum accuracy one could hope for from the data available.

C. *Long-Range Effects*

For many potentials the wavefunction is non-negligible over a large range of long and short distances. If the tabulated points do not contain sufficiencly long- or short-range values, then it is necessary to extrapolate those values in some way. The effects of the extrapolation form on the eigenvalues obtained will now be assessed.

One form of extrapolation which has been used in scattering calculations is an inverse power form

$$V = Ar^{-a} \tag{14}$$

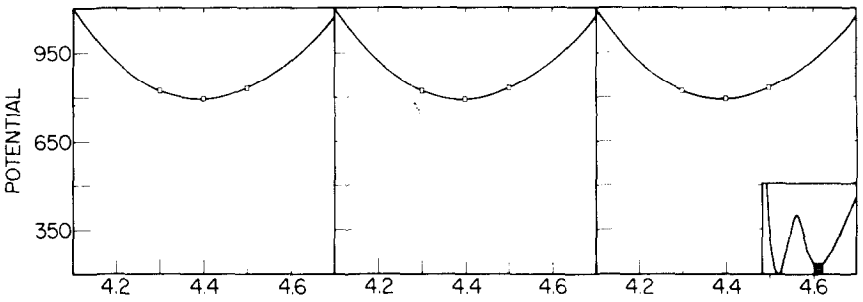

FIG. 5. The interpolated outer minimum of the Kołos and Wolniewicz $E, F^1\Sigma_g$ potential of H_2. Shown are Lagrangian (left panel), Hermite (center), and spline (right) interpolation. Both third and fifth oder functions were used. The two fits are indistinguishable in all cases. Fifteen points clustered around the extrema have been deleted, as described in the text. The tabulated points are shown as □. The shaded box within the small insert shows the location of these panels within the potential. The potential is given in units of cm^{-1}.

where A and a (> 0) are determined by the values of the outermost two tabulated points. A second form, and one more appropriate to the Morse potential, is

$$V = Be^{-br}, \tag{15}$$

where B and b are determined in the same way as A and a above. A second approach uses the "correct" asymptotic form for the potential. In the case of real intermolecular potentials this form will be a sum of integer inverse powers of r

where the C_n's are determined from empirical multipole moments, polarizability, and hyperpolarizabilities. For intramolecular potentials, the situation is often more complicated, and exchange forces may dominate even at large distances, especially for molecules in excited electronic states [23]. This leads to a form different from Eq. (16). In the case of the Morse potential, Eq. (12), the asymptotic form can be extracted to give

$$V = 4 - 8e^{-r/2}. \tag{17}$$

In the following third and fifth order spline interpolation will be examined, and the results compared to ensure that the effects of interpolation have been eliminated. The results of these calculations are reported in Tables VII and VIII, which contain the

TABLE VII

Eigenvalues for Spline Interpolated Morse Potential Points Matched to Various Long-Range Forms at $r = 4$[a]

v	Exact Morse form	Asymptotic form[b]	Asymptotic form[c]	Matched exponential	Matched inv. power
0	0.93748367[d]	0.93747930	0.93748267	0.93748343	0.93748201
	0.93750003	0.93749567	0.93749912	0.93749979	0.93749837
1	2.43748835	2.43673365	2.43725246	2.43742253	2.43700406
	2.43750002	2.43674756	2.43727826	2.43743425	2.43701611
2	3.43749301	3.42585684	3.43166602	3.43485503	3.41505281
	3.43750001	3.42589812	3.43189253	3.43486250	3.41506262
3	3.93749764	3.93452026	3.93439778	3.92769455	3.94888913
	3.93750000	3.93452294	3.93445118	3.92769694	3.94888970

[a] The central region is an interpolation on 25 equispaced points. Eigenvalues are in the reduced units of Eq. (1).

[b] The form is $V(r) = 4 - 8e^{-r/2}$, where the interpolation is performed on the region from $r = -2$ to $r = 4$, with two additional points at $r = 4.25$ and $r = 4.5$.

[c] Same form as above, but with additional point located at $r = 5$ and $r = 6$.

[d] Upper number is for third order spline interpolation, while the lower is for fifth order.

TABLE VIII

Eigenvalues for Spline Interpolated Morse Potential Points Matched to Various Long-Range Forms at $r = 6$[a]

v	Exact Morse form	Asymptotic form[b]	Asymptotic form[c]	Matched exponential	Matched inv. power
0	0.93748367[d]	0.93748366	0.93748367	0.93748367	0.93748367
	0.93750003	0.93750002	0.93750003	0.93750003	0.93750002
1	2.43748835	2.43748691	2.43748795	2.43748825	2.43748691
	2.43750002	2.43749858	2.43749964	2.43749992	2.43749858
2	3.43749302	3.43725186	3.43739554	3.43745857	3.43696890
	3.43750001	3.43725956	3.43740591	3.43746557	3.43697605
3	3.93749765	3.93616613	3.93659095	3.93653437	3.91835129
	3.93750000	3.93617137	3.93661342	3.93653674	3.91835366

[a] The central region is an interpolation of 33 equispaced points. Eigenvalues are in reduced units of Eq. (1).

[b] The form is $V(r) = 4 - 8e^{-r/2}$, where the interpolation is performed on the region from $r = -2$ to $r = 6$, with two additional points at $r = 6.25$ and $r = 6.5$.

[c] Same form as above, but with additional point located at $r = 7$ and $r = 8$.

[d] Upper number is for third order spline interpolation, while the lower is for fifth order.

eigenvalues for potentials with the various long-range forms described above. In all cases the short-range form is the exact Morse oscillator potential. In Table VII the potential is interpolated between $r = -2$ and $r = 4$, with the long-range form beyond, while in Table VIII the interpolated region is between $r = -2$ and $r = 6$. For the asymptotic form, if the interpolation and long-range form do not overlap regions, then a discontinuity will result at the joining point. A remedy is to interpolate the set of discrete points for the Morse function plus two more for the asymptotic values, thus joining them smoothly. The two extra points are chosen in one of two ways—the two points may be chosen such that the separation between them is the same as between any other two points, or the points may be chosen farther apart, so as to smooth the joining even more. These results are shown in clumns 2 and 3, respectively, in Tables IX and X. In column 3 the results are for the potential, where this separation is 1 reduced unit.

The information in Tables VII and VIII is not easily interpretable, since it is not clear how the source of the error is distributed between interpolation and extrapolation. Therefore Tables IX and X present the percentage error in each column of Tables VII and VIII, respectively. The excellent agreement between the third and fifth order spline results indicates that the error shown is due to extrapolation alone.

With increasing eigenvalue the error increases, which is the opposite of what is observed for interpolation error. This is to be expected since the wavefunctions for

TABLE IX

Percentage Error in Eigenvalues Due to Extrapolation of Spline Interpolated Morse Potential Points[a]

v	Asymptotic form[b]	Asymptotic form[c]	Matched exponential	Matched inv. power
0	$-4.661-4$[d]	$-1.067-4$	$-2.560-5$	$-1.771-4$
	$-4.651-4$	$-9.707-5$	$-2.560-5$	$-1.771-4$
1	$-3.096-2$	$-9.678-3$	$-2.700-3$	$-1.987-2$
	$-3.087-2$	$-9.098-3$	$-2.698-3$	$-1.985-2$
2	$-3.385-1$	$-1.695-1$	$-7.674-2$	$-6.528-1$
	$-3.375-1$	$-1.631-1$	$-7.673-2$	$-6.527-1$
3	$-7.562-2$	$-7.873-2$	$-2.490-1$	$2.893-1$
	$-7.561-2$	$-7.743-2$	$-2.490-1$	$2.893-1$

[a] Percentage error calculated as $100(x-y)/y$, where y is the entry in the first column of Table VII, and x is the entry from the appropriate long-range form (see text). The potential is matched to various long-range forms at $r=4$.

[b] The form is $V(r)=4-8e^{-r/2}$, where the interpolation is performed on the region from $r=-2$ to $r=4$, with two additional points at $r=4.25$ and $r=4.5$.

[c] Same form as (b), but with additional points located at $r=5$ and $r=6$.

[d] Upper number is for third order spline interpolation, while the lower is for fifth order. The trailing signed integer is the power of 10 to be multiplied by the entry.

higher eigenvalues extend farther into the long-range part of the potential, and are thus more affected by errors there.

The inverse power extrapolation gives the worst results in this case, as expected, and will not be considered further. The remaining forms all have the correct, i.e., exponential, asymptotic behavior. In columns 1 and 2 of Tables VII and VIII, marked "asymptotically correct," the potential becomes $4-8e^{-r/2}$ at long range, which is exact in the limit of large r, but incorrect for shorter distances. In column 3 the matched exponential form is used and the potential is correct at short distances beyond the joining point, but has the wrong exponential dependence for large distance. The difference in columns 1 and 2 reflects an attempt to make the transition smoother, as described above, for the potential of column 2. Of course, the matched exponential will approach the asymptotic value as the matching point is moved out. Thus better results are obtained in Table X for both the matched and asymptotic exponential cases.

IV. Summary and Conclusions

Several conclusions can be drawn from the results presented here. For numerical solution of the Schrödinger equation with bound state boundary conditions, the

TABLE X

Percentage Error in Eigenvalues Due to Extrapolation of Spline Interpolated Morse Potential Points[a]

v	Asymptotic form[b]	Asymptotic form[c]	Matched exponential	Matched inv. power
0	$-1.067-6$[d]	$<1.0-6$[e]	$<1.0-6$	$<1.0-6$
	$-1.067-6$	$<1.0-6$	$<1.0-6$	$-1.067-6$
1	$-5.908-5$	$-1.641-5$	$-4.103-6$	$-5.908-5$
	$-5.908-5$	$-1.559-5$	$-4.103-6$	$-5.908-5$
2	$-7.016-3$	$-2.836-3$	$-1.002-3$	$-1.525-2$
	$-6.995-3$	$-2.737-3$	$-1.002-3$	$-1.524-2$
3	$-3.382-2$	$-2.303-2$	$-2.446-2$	$-4.863-1$
	$-3.374-2$	$-2.252-2$	$-2.446-2$	$-4.863-1$

[a] Percentage error calculated as $100(x-y)/y$, where y is the entry in the first column of Table VIII, and x is the entry from the appropriate long-range form (see text). The potential is matched to various long-range forms at $r=6$.

[b] The form is $V(r)=4-8e^{-r/2}$, where the interpolation is performed on the region from $r=-2$ to $r=6$, with two additional points at $r=6.25$ and $r=6.5$.

[c] Same form as (*b*), but with additional points located at $r=7$ and $r=8$.

[d] Upper number is for third order spline interpolation, while the lower is for fifth order. The trailing signed integer is the power of 10 to be multiplied by the entry.

[e] Entries agree to accuracy reported.

Numerov–Cooley method is the most efficient of those examined here when the potential is easily evaluated. In situation where multiple minima exist, or the potential evaluation requires a great computational effort, FEM is easier to use than Numerov–Cooley, and is superior to the other matrix methods discussed herein.

Interpolation of a priori data points for potentials must be made with extreme care. Although higher order polynomial interpolates are accurate for accurate data, they are very unpredictable with noisy data. The higher order spline functions are particularly dangerous in this respect. It is always wise to plot the fits and visually inspect them before using them and to try several different fits to obtain an indication of the accuracy obtainable with the data. Many closely spaced points in a particular region of the potential tend to exaggerate noise in the interpolated function, and the fitted points should be selected judiciously. The higher eigenvalues appear to be less sensitive to the interpolation.

The long-range form of the potential also effects the eigenvalues. In this case it is the higher eigenvalues which are most likely to be affected; they correspond to states with classical turning points closer to the long-range region. If in the matching procedure any lack of smoothness is introduced into the potential, the eigenvalues nearest the joining will be most affected.

APPENDIX A: NATURAL COORDINATES AND LAGRANGIAN INTERPOLATES

The basis functions used for evaluation of the finite element integrals over elements are best formulated in a local rather than global coordinate system. This approach allows the integrals to be evaluated over an arbitrary element and then readily assembled into the complete system given by Eqs. (6)–(8). Since these functions satisfy the property of Eq. (9), interelement continuity is automatically assured.

For the following discussion, we assume that elemetns are of equal size with primary spacing h. Let r_i and r_j be the initial and final global coordinate specifying the element ($h = r_j - r_i$). We choose the local coordinates

$$L_i(r) = (r_j - r)/h \tag{18}$$

and

$$L_j(r) = (r - r_i)/h. \tag{19}$$

Clearly these coordinates satisfy the condition on interpolates that $L_i(r_k) = \delta_{ik}$ with $k = i$ or j. An arbitrary global point r can be specified in terms of L_i and L_j by

$$r = L_i r_i + L_j r_j \tag{20}$$

It is easy to see that $L_i + L_j = 1$ from Eqs. (18) and (19). Since the global system is one dimensional, two coordinates overspecify the system. However, the symmetry afforded by this construct is useful in the application of the interpolates. We observe that L_i is zero at $r = r_j$ while L_j is unity there; and L_i is unity at $r = r_i$ while L_j is zero there. We further observe that the linear coordinates L_i and L_j are actually linear Lagrangian interpolation functions.

Since derivatives of the interpolation functions are required for the energy integrals H_{ij} of Eq. (7), they may be readily given by

and

$$dL_j/dr = 1/h. \tag{22}$$

Since all higher order Lagrangian interpolates will simply be polynomials of the local coordinates, the following integration formula facilitates such evaluations:

$$\int L_i^p L_j^q \, dr = p!\, q!\, h/(p + q + 1)!. \tag{23}$$

The specification of higher order Lagrangian interpolates can easily be determined following a procedure outlined by Silvester [8]. The approach generates any order (or

degree) n Lagrangian interpolate as a function of local coordinates. The interpolate is designated by the product function $N_{ab}(L_i, L_j)$, where $a + b = n$, and given by

$$N_{ab}(L_i, L_j) = \mathcal{N}_a(L_i)\,\mathcal{N}_b(L_j), \tag{24}$$

where

$$\begin{aligned} \mathcal{N}_a(L_i) &= \prod_{k=1}^{a} \frac{(nL_i - k + 1)}{k}, \qquad a > 0, \\ &= 1, \qquad a = 0, \end{aligned} \tag{25}$$

and similarly for $\mathcal{N}_b(L_j)$. For example, for quadratic interpolates $n = 2$; ab can be 20, 02, or 11. The 20 and 02 functions correspond to primary interpolates and 11 to secondary interpolates. They are written

$$\begin{aligned} \text{primary:} \quad & N_{20} = L_i(2L_i - 1), \\ \text{secondary:} \quad & N_{11} = 4L_iL_j, \\ \text{primary:} \quad & N_{02} = L_j(2L_j - 1). \end{aligned}$$

Again it is clear (see Fig. 6) that these interpolates satisfy the Eq. (9) condition; e.g.,

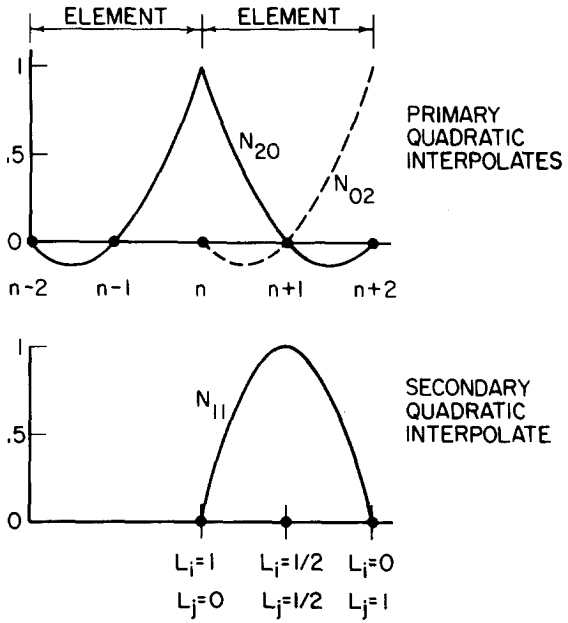

FIG. 6. Quadratic interpolates and natural coordinates. The primary interpolate associated with node n is given in the upper figure. The secondary associated with node $n + 1$ is given in the lower figure. For a given element (between nodes n and $n + 2$), there are three interpolates: the primary branches N_{20} and N_{02} and the secondary interpolate N_{11}. It is clear from the figure that at a node only a single interpolate is non-zero.

N_{20} is unity at $L_i = 1$ and zero at the remaining two nodes, $L_i = \frac{1}{2}$ and 0 (or equivalently $L_j = \frac{1}{2}$ and 1). The primary functions N_{20} and N_{02} extend into adjacent elements, but are defined by the nodes in the respective elements. The secondary interpolate N_{11} is only non-zero in the element containing it. In global coordinates, these functions are less concise. For example, for equally spaced elements we have

$$\begin{aligned} N_{20} &= \left(\frac{r - r_i + h}{h}\right)\left[2\left(\frac{r - r_i + h}{h}\right) - 1\right], && r_i - h < r < r_i, \\ &= \left(\frac{r_j - r}{h}\right)\left[2\left(\frac{r_j - r}{h}\right) - 1\right], && r_i \leqslant r \leqslant r_j, \\ &= 0, && r > r_j, \quad r < r_i - h. \end{aligned}$$

Since the primary node at r_i is shared by two elements, the interpolate for $r_i < r < r_j$ is different from that in the element preceding it ($r_i - h < r < r_i$). The interpolate is identically zero outside these two elements.

Cubic Lagrangian interpolates (used in the calculations here) can be given using the above scheme by

$$\begin{aligned} \text{primary:} \quad & N_{30} = \tfrac{1}{2}L_i(3L_i - 1)(3L_i - 2), \\ \text{secondary:} \quad & N_{21} = \tfrac{9}{2}L_iL_j(3L_i - 1), \\ \text{secondary:} \quad & N_{12} = \tfrac{9}{2}L_iL_j(3L_j - 1), \\ \text{primary:} \quad & N_{03} = \tfrac{1}{2}L_j(3L_j - 1)(3L_j - 2). \end{aligned}$$

All of the interpolates satisfy sum rules which can be used to check integration results over an element. In particular,

$$\sum_k N_k = 1, \tag{26}$$

and

$$\sum_k N'_k = 0, \tag{27}$$

where the sums are over all nodes of a particular element.

APPENDIX B: An Algorithm for the Solution of the Symmetric Banded Generalized Eigenvalue Problem

The FEM approach reduces the Schrödinger equation to a generalized algebraic eigenvalue problem

$$(\underline{\mathbf{H}} - E_v\underline{\mathbf{S}})\,\underline{\mathbf{X}}_v = \underline{\mathbf{0}}, \tag{28}$$

where $\underline{\mathbf{H}}$ and $\underline{\mathbf{S}}$ are as previously defined. E_v is an eigenvalue, and $\underline{\mathbf{X}}_v$ is its associated eigenvector. It is important to note that both $\underline{\mathbf{H}}$ and $\underline{\mathbf{S}}$ are symmetric and banded,

with a bandwith of order $2m + 1$, where m is the order of the Lagrangian interpolates employed. While methods do exist for the generalized eigenvalue problem which make use of the symmetry of the matrices, these destroy the band structure of the matrices, increasing computation time and storage requirements. These methods turn the generalized eigenvalue problem into a regular eigenvalue problem with *full* symmetric matrices. The use of these methods for large numbers of elements is prohibitive, in terms of both time and storage requirements. Thus it is more efficient to use the following iterative approach.

If an approximate eigenvalue e_v is known, it can be used to form the operator,

$$\mathbf{G}(e_v)\,\mathbf{S} = (\mathbf{H} - e_v\mathbf{S})^{-1}\,\mathbf{S}. \tag{29}$$

Applying this to an arbitrary vector,

$$\mathbf{v}_{n;v} = \sum_{v'} \mathbf{X}_{v'} a_{n;v',v}, \tag{30}$$

produces

$$\begin{aligned}\mathbf{G}(e_v)\,\mathbf{S}\mathbf{v}_{n;v} &= \sum_{v'} \mathbf{X}_{v'} a_{n;v',v}/(E_{v'} - e_v) \\ &= c \sum_{v'} a_{n+1;v',v}\mathbf{X}_{v'},\end{aligned} \tag{31}$$

where c is a normalization constant. $\mathbf{v}_{n;v}$ can now be identified as the nth approximation to $\mathbf{X}_v$ in the iteration scheme, Eq. (31). It is convenient for purposes of this method to use a supremum norm,

$$\|\mathbf{v}_{n;v}\| = \sup(v_{n;v,j}) = 1, \tag{32}$$

the largest element of $\mathbf{v}_{n;v}$. If e_v is such that

$$|E_v - e_v| \ll |E_{v'} - e_v|, \qquad v \neq v', \tag{33}$$

then $\mathbf{v}_{n+1;v}$ is a better approximation to $\mathbf{X}_v$ than was $\mathbf{v}_{n;v}$. After a few iterations $\mathbf{v}_{n;v}$ is very close to $\mathbf{X}_v$, and

$$1/c = E_v - e_v, \tag{34}$$

or,

$$E_v = e_v + 1/c. \tag{35}$$

In practice, the e_v's and $\mathbf{v}_{0;v}$'s are obtained from a low-accuracy calculation using direct matrix diagonalization methods, and stored on disk. Only one vector need be present in core at any one time. The vector is improved by iteration, and is then written back to disk. Each iteration requires one (banded) matrix multiplication, $\mathbf{S}\mathbf{v}_{n;v}$, and the solution of the banded system of equations,

$$c(\mathbf{H} - e_v\mathbf{S})\,\mathbf{v}_{n+1;v} = \mathbf{S}\mathbf{v}_{n;v}. \tag{36}$$

This is done using a variant of the LU decomposition method [24] which requires the storage of only one of the triangular factors, which will have the same band structure as the original matrix. This method is described in Appendix C. Since the left-hand-side matrix $(\underset{\sim}{H} - e_v\underset{\sim}{S})$ does not change from iteration to iteration, the decomposition is performed only once, and the solution of the system of equation reduces to a forward and a backward substitution for each iteration. The initial guess $\mathbf{v}_{0;v}$ must be obtained for each eigenvector. Although with a good initial guess to the eigenvalue an arbitrary vector would eventually produce the correct answer, the closer the initial guess is to the proper vector the fewer iterations are required. The eigenvectors read in from the results of the crude first guess have fewer points than are needed for the refined guess, so an interpolation procedure is needed. As was shown in Section II, spline function interpolation seems to minimize the error in the wavefunction between known points, and thus is used here to produce the wavefunction at all necessary points.

APPENDIX C: AN EFFICIENT ALGORITHM FOR THE SOLUTION OF BANDED SYMMETRIC MATRIX EQUATIONS

Consider the matrix equation,

$$\underset{\sim}{A}\mathbf{X} = \mathbf{B}, \tag{37}$$

where $\underset{\sim}{A}$ is a symmetric real valued banded matrix. If this equation has to be solved for a particular $\underset{\sim}{A}$ and a number of $\mathbf{B}$'s it is useful to decompose $\underset{\sim}{A}$ into triangular factors, and solve two related equations, which may be done more easily. In particular, since $\underset{\sim}{A}$ is symmetric, the factors may be chosen such that

$$\underset{\sim}{A} = \underset{\sim}{S}'\underset{\sim}{S}. \tag{38}$$

It is well known that this produces an upper and a lower triangular matrix, each with the same half bandwidth as $\underset{\sim}{A}$. If, however, $\underset{\sim}{A}$ is not positive definite, then some of the elements of $\underset{\sim}{S}$ may be pure imaginary.

The matrix $\underset{\sim}{S}$ can be easily generated by a set of recursion relations [24],

$$\begin{aligned}
&s_{11} = a_{11}^{1/2}, \\
&s_{1j} = a_{1j}/s_{11}, \\
&s_{ii} = \left(a_{ii} - \sum_{k=1}^{i-1} s_{ki}^2\right)^{1/2}, \\
&s_{ij} = \left(a_{ij} - \sum_{k=1}^{i-1} s_{ki}s_{kj}\right)\Big/ s_{ii} \qquad (j > i), \\
&s_{ij} = 0 \qquad (i > j).
\end{aligned} \tag{39}$$

It is easy to see from Eq. (39) that any row of $\underset{\sim}{S}$ is either pure real or pure imaginary.

Real valued matrices can be produced by the use of a diagonal matrix $\underset{\sim}{D}$, such that $d_{ii} = 1$ if s_{ij} is real, and $d_{ii} = i$ if s_{ij} is imaginary. Note that $\underset{\sim}{D}^4 = I$, the identity, and so,

$$\underset{\sim}{A} = \underset{\sim}{S}^t\underset{\sim}{S} = \underset{\sim}{S}^t\underset{\sim}{D}^4\underset{\sim}{S} = (\underset{\sim}{S}^t\underset{\sim}{D}^3)\,\underset{\sim}{D}\underset{\sim}{S}. \tag{40}$$

Defining $\underset{\sim}{L} = \underset{\sim}{S}^t\underset{\sim}{D}^3$ and $\underset{\sim}{U} = \underset{\sim}{D}\underset{\sim}{S}$, Eq. (40) becomes

$$\underset{\sim}{A} = \underset{\sim}{L}\underset{\sim}{U}. \tag{41}$$

$\underset{\sim}{U}$ is easily produced from Eq. (39) by setting $u_{ij} = s_{ij}$ if s_{ij} is real, and $u_{ij} = -|s_{ij}|$ if s_{ij} is imaginary. Only $\underset{\sim}{U}$ need be calculated and stored since the elements of $\underset{\sim}{L}$ are easily generated from

$$L_{ij} = \operatorname{sgn}(u_{ii})\,u_{ij}, \tag{42}$$

where $\operatorname{sgn}(x)$ is the algebraic sign of x.

Now Eq. (37) can be written as a combination of two matrix equations,

$$\underset{\sim}{L}\underset{\sim}{Z} = \underset{\sim}{B}, \tag{43}$$

and

$$\underset{\sim}{U}\underset{\sim}{X} = \underset{\sim}{Z}. \tag{44}$$

Each can be efficiently solved by substitution, since both $\underset{\sim}{L}$ and $\underset{\sim}{U}$ are triangular matrices.

ACKNOWLEDGMENTS

The authors would like to thank the referees for their detailed and thoughtful comments on the manuscript.

REFERENCES

1. (a) B. G. WICKE AND D. O. HARRIS, *J. Chem. Phys.* **64** (1976), 5236; (b) D. O. HARRIS, G. O. ENGERHOLM, AND W. GWINN, *J. Chem. Phys.* **43** (1965), 1515.
2. W. KOLOS AND L. WOLNIEWICZ, *J. Chem. Phys.* **50** (1969), 3228.
3. D. G. TRUHLAR AND W. D. TARARA, *J. Chem. Phys.* **64** (1976), 237.
4. J. K. CASHION, *J. Chem. Phys.* **39** (1963), 1872.
5. D. G. TRUHLAR, *J. Comput. Phys.* **10** (1972), 123.
6. D. G. TRUHLAR, "Numerical Eigenvalues and Matrix Elements for the Quantum Mechanical Radial Equation," Program 203, Quantum Chemistry Program Exchange, Indiana University, 1972.
7. B. W. SHORE, *J. Chem. Phys.* **59** (1973), 6450.
8. K. H. HUEBNER, "The Finite Element Method for Engineers," Wiley, New York, 1975.
9. D. H. NORRIE AND G. DEVRIES, "An Introduction to the Finite Element Method," Academic Press, New York, 1978.

10. A. ASKAR, *J. Chem. Phys.* **62** (1975), 732.
11. S. NORDHOLM AND G. BACSKAY, *Chem. Phys. Lett.* **42** (1976), 253.
12. S. NORDHOLM AND G. BACSKAY, *Chem. Phys. Lett.* **42** (1976), 259.
13. A. ASKAR, A. C. CAKMAK, AND H. A. RABITZ, *Chem. Phys.* **33** (1978), 267.
14. M. FRIEDMAN, Y. ROSENFELD, A. RABINOVITCH AND R. THIEBERGER, *J. Comput. Phys.* **26** (1978), 9169.
15. G. STRANG AND G. J. FIX, "An Analysis of the Finite Element Method," Prentice–Hall, Englewood Cliffs, N. J., 1973.
16. P. M. PRENTER, "Splines and Variational Methods," Wiley–Interscience, New York, 1975.
17. Two program packages have been submitted to QCPE at Indiana University. COOLEY is a self-starting Numerov–Cooley program, and FEM1D consists of a package of two programs and related subroutines. FEM1DC is a direct-method finite element program, using cubic Lagrangian interpolates, and designed to perform small-scale calculations. XFEM1D utilizes the iterative procedure described here to refine the FEM1DC calculations to the results for a larger number of nodes. Both programs are in Program 407 of OCPE.
18. D. SECREST, in preparation
19. A. TALMI AND G. GILAT, *J. Comput. Phys.* **23** (1977), 93.
20. C. S. LIN, *J. Chem. Phys.* **60** (1974), 4660.
21. P. L. TOBIN AND J. HINZE, *J. Chem. Phys.* **65** (1976), 1654.
22. L. WOLNIEWICZ AND T. ORLIKOWSKI, *J. Comput. Phys.* **27** (1978), 169.
23. R. S. MULLIKEN, *Phys. Rev.* **120** (1960), 1674.
24. D. K. FADDEEV AND V. N. FADDEEVA, "Computational Methods of Linear Algebra," W. H. Freeman, San Francisco, 1963.